Imaging a buried terrane with district-scale ambient noise tomography and gravity modelling: insights for scale-reduction in mineral exploration

Anthony Reid[1,2], Nicholas Smith[1], Adebayo Ojo[1], Stephen Barber[1], Doug Menzies[3], Gerrit Olivier[1,4],

[1] Fleet Space Technologies, Beverley, South Australia.

[2] Department of Earth Sciences, The University of Adelaide, Adelaide, South Australia.

[3] Inflection Resources, 1210-1130 West Pender Street, Vancouver, BC V6E 4A4, Canada

[4] Centre for Ore Deposits and Earth Sciences, University of Tasmania, TAS, Australia

Abstract

Mineral exploration proceeds by a process of scale-reduction. Decisions need to be made at all stages as the physical search space becomes progressively reduced from regional through to district, camp and tenement/deposit scale. While there are many regional scale datasets available to explorers through public geoscience agencies, one of the most difficult steps to make is from the regional-scale down to the district- and camp-scale, particularly in areas with post-mineral cover. Three dimensional models of subsurface geology at the district- to camp-scale can provide a means to filter for areas of enhanced prospectivity, for example by looking for broad structural or lithological features that are favourable for mineralisation. For the most part, 3D models of subsurface geology are developed by relying on inversions of potential field data coupled with other constraints such as surface mapping, drilling, electrical geophysics and, if available, reflection seismic data. Passive seismic methods are less commonly used by the exploration industry as a means to image subsurface geology, despite the method being able to provide depth-constrained, three dimensional seismic velocity information that is complementary to potential field data. As an example of the use of a district-scale passive seismic array to image the upper crust and architecture of possible mineral systems, we present a 3D velocity model derived from an ambient noise tomography (ANT) survey across an area of 1,800km^2 in the northern Macquarie Arc under >100m of Mesozoic to Cenozoic cover. The ANT velocity model extends to depths of ~5km and reveals velocity features that are ~1-1.5 km thick and are spatially correlated with granitic plutons evident in potential field data. These larger, apparently magmatic bodies may represent multi-stage granitic plutons, and could represent source zones for possible magmatic-associated hydrothermal mineralisation. The ANT model also clearly delineates the steep, westerly dip on a major shear zone that runs through the centre of the survey area. When this type of ANT velocity model is available and combined with potential field data, exploration decisions can proceed with more confidence since they are based on consideration of multiple petrophysical properties - density, magnetism and velocity.

Key words: geophysical methods, passive seismic, mineral exploration, inversion modelling

Introduction

Mineral systems are an outcome of the combination of geological fertility, geodynamics and lithospheric architecture, with preservation also playing a role in capacity for discovery of ore bodies (see for example Groves et al., 2022, and related publications). Geophysical data is an important constraint on the crustal and indeed lithospheric architecture within which mineral systems form, as it is able to image pathways through which fluid and magma may have travelled (Heinson et al., 2018). Understanding mineral potential, at least in a conceptual sense, can be improved by accurately imaging features in the subsurface that can be related to the style of mineral deposit and the related fertility and geodynamic features that are of interest.

One of the challenges for holistic conceptual analysis of the subsurface is the varying scales at which the geophysical observations are made. For example, in countries such as Australia, Canada, United States and elsewhere, government initiatives have delivered a raft of deep crustal reflection seismic surveys, ambient noise tomography and also magnetotelluric surveys that provide constraints on the entire crust and upper mantle at the regional scale (e.g. Clowes et al., 2005; Hammer et al., 2010; Kirkby et al., 2020; O'Donnell et al., 2023). At the other end of the spectrum, individual mineral exploration companies undertake surveys at the tenement scale, often as a means to determine 'anomalies' that can be tested via drilling. Perhaps only government potential field data, such as aeromagnetics, truly covers large areas at reasonably high resolution (<400m line spacing for example), although exploration companies typically fly their own, more detailed aeromagnetic surveys as follow up.

This variation in scale of geophysical data also mirrors the general process of mineral exploration in which the first step is to determine the area of interest at a regional scale (Fig. 1). Then within the region, select a district of interest before proceeding to identify camp and tenement-scale areas of interest, for further data collection, drilling and ideally discovery. One of the challenges for the scale-reduction process in exploration is there is often a systematic gap in observational datasets between regional to camp/tenement scale. While regional datasets provide wide areas of interest (Hoggard et al., 2020), the next scale of geophysical data with which to make informed decisions about where in a region is most prospective may be lacking.

In this paper, we present the results of a district-scale ambient noise tomography survey across buried Ordovician - Devonian rocks in central New South Wales, Australia (Fig. 2). This survey represents the largest ANT survey dedicated to mineral exploration that we are aware of, covering ~1,800 km2 with a strike length of ~150 km and maximum width of ~40 km. This survey is a unique opportunity to visualise the upper 5 km of the crust in this region at a scale that is intermediate between the regional and continental scale seismic velocity data (O'Donnell et al., 2023), and camp and tenement scale surveys undertaken by individual exploration companies (Jones et al., 2024). The district-scale ANT velocity model has clear correlations with features evident in potential field data including major structures. We discuss the model in

the context of depth inversions of government gravity data which provides additional constraints on the subsurface geology. This scale of survey lends itself to area selection for further exploration based on the type of mineral system of interest.

Geological setting

The district-scale ANT survey was conducted in a region of the northern Macquarie Arc, New South Wales, within the northern extension of the Junee – Narromine Volcanic Belt. The survey lies within contiguous tenements of a single exploration company, Inflection Resources, a land holding that has enabled the deployment of a survey at such a broad scale (Fig. 2). The Macquarie Arc hosts a range of magmatic related mineral deposits including porphyry Cu-Au, epithermal and skarn-type, along with structurally controlled Au-Cu deposits (Holliday et al., 2002; Chalmers et al., 2007; Cooke et al., 2007; Squire et al., 2007; Kreuzer et al., 2015). The Macquarie Arc formed as an intra-oceanic volcanic arc that developed on oceanic crust via west-dipping subduction (Crawford et al., 2007b; Glen et al., 2007, 2012; Fergusson, 2009). Magmatism in the Macquarie Arc spanned early shoshonitic and high-K calc-alkaline style volcanism towards more dacitic and finally a series of variably mineralised monzonitic to monzodioritic intrusions, the latter of which typically span the age range c. 440-437 Ma (Dwyer et al., 2025). This final phase is interpreted to have occurred in a post-collisional extensional setting which was triggered by perturbation of subduction and subsequent slab rollback (Glen et al., 2007, 2011). The Ordovician arc system was subsequently dismembered via strike slip and extensional tectonics, as well as a series of younger rift basins that overly and surround the arc segments (Glen et al., 2012).

The Macquarie Arc is partly buried beneath a series of basins, including Permo-Triassic rocks in the east (Gunnedah Basin) and Mesozoic sediments of the Great Artesian Basin in the north. Cenozoic volcanism in the form of largely basaltic shield volcanoes and lava fields occur across eastern Australia including the Macquarie Arc (Rawlinson et al., 2017). Post-Miocene sediment also provides a thin veneer across the region.

Geology of the survey area

The survey area is entirely buried beneath Mesozoic and younger, predominantly alluvial sediment (Fig. 3a). The Ordovician rocks of the Junee - Narromine Volcanic Belt constitute basaltic and andesitic volcanics and associated volcaniclastic sedimentary rocks (Glen et al., 2003)Narromine Igneous Complex; (Glen et al., 2003). The Ordovician units are intruded by a range of felsic to mafic bodies that formed from the Late Ordovician into the Devonian. Overlying Silurian sedimentary rocks are present as narrow basins that overly these dominantly igneous rock packages, and are filled with carbonate and or siliciclastic sediment related to the Derriwong, Waugoola and Mumbil groups that occur across the region (Groome et al., 2021). Localised deposits of Devonian terrigenous to shallow marine quartzose to lithic sandstone, siltstone, shale are present in the area (Sherwin, 1996)e.g. Hervey Group; (Sherwin, 1996)

Aeromagnetic images delineate the extent of the Ordovician - Devonian igneous intrusive bodies through the central region of the survey area, which appear to intrude into smaller, generally linear high magnetic intensity features (Fig. 3c). The survey area runs approximately parallel to a discontinuity seen in magnetic data that reflects a north-northwest trending shear zone that anastomoses along several splays most clearly defined in the southern area of the survey (Fig. 3c). In the southern area, magnetic features of intrusive bodies terminate against the shear zone, suggesting the shear zone is younger than the intrusions. Zones of very low magnetic intensity occur either side of this shear zone that overprint the variably magnetic textured intrusions and correlate with Silurian sedimentary rocks.

The gravity signal across the survey area is characterised by a ridge of high gravity that runs in a north-westerly orientation, that separates two similarly oriented ridges of lower gravity response (Fig. 3d). In detail, some of the intrusive features of the area are associated with subtle gravity lows that sit above zones of intermediate gravity, while others, particularly in the east of the area the gravity lows are more prominent and stronger.

Intersections of basement rock from the limited diamond drill holes across the survey area are consistent with the presence of intrusive bodies into volcanic and volcaniclastic rocks, as is typical for other portions of the Macquarie Arc (Menzies et al., 2024). For example, drill hole TD02 in the south of the survey area (Fig. 3c) contains pyroxene magnetite- and hornblende-bearing porphyry that intrudes andesite and basaltic andesite (Hughes, 1998). Likewise, drill holes with prefix ACDNY- in the northwest of the survey area contain volcaniclastic siltstone, sandstone and conglomerate, basalt and andesite (Fitzpatrick, 2005).

U-Pb zircon ages from monzogabbro, monzodiorite and monzonite intrusions rocks to the immediate south of the study area have emplacement ages c. 466 – 460 Ma, while hornblende gabbro, diorite and granodiorite, and including quartz + plagioclase + hornblende-phyric dacitic porphyries were emplaced at c. 445 Ma (Crawford et al., 2007a). Devonian intrusions are also known in the area with granites having ages c. 395 Ma (Watkins and Meakin, 1996).

Methods

ANT survey and velocity model construction

ANT is a passive technique using vibrations generated by earthquakes, weather, ocean movements and anthropogenic sources. ANT utilises the cross-correlation of random wavefields recorded at multiple seismic sensors to approximate elastodynamic Green's functions between pairs of receivers (Shapiro et al., 2005; Bensen et al., 2007). Each receiver effectively tracks surface waves travelling between it and every other receiver in the array across a range of frequencies, resulting in a velocity model of the subsurface since the travel time is a result of the variable seismic impedance of the subsurface.

The ANT system deployed in this study utilises seismic sensors called Geodes developed by Fleet Space Technologies (Olivier et al., 2022). Geodes utilise high-sensitivity 2 Hz geophone elements, alongside high-gain and low-noise digitiser which enable us to reliably extract surface waves from ambient noise at frequencies as low as 0.1 Hz. The increased sensitivity at low frequency enables us to use Geodes across multiple scales in the scale reduction process in mineral exploration. The Geodes are part of the exploration suite, ExoSphere by Fleet®, and are designed with an increased sensitivity to low-frequency signals, reducing data gathering time compared to conventional nodal geophones and are equipped with a real-time direct-to satellite Internet of Things (DtS-IoT) modem and edge processing capabilities, enabling rapid data transmission for cloud-based processing.

A network of 100 Geodes were deployed over the survey area with a nominal spacing of 5km, over an area of 1,800km2 for 10 days to allow recovery of sufficient signal across the frequencies of interest. Continuous ambient seismic noise data was recorded at a 20 Hz sampling rate. As part of the Geode capability, edge processing was applied to enhance and compress the data prior to transmission via satellite to the cloud. The edge processing steps applied consist of a) amplitude clipping - to reduce the impact of high amplitude transient signals, b) spectral whitening - to normalise the seismic energy in the frequency band of interest (0.1 - 9 Hz) and c) one-bit normalisation - to achieve a 32x data compression and further reduce unwanted transient signals. The pre-processed data were promptly transmitted to the cloud for real time processing, generating preliminary 3D models every 6 h. Throughout the deployment, satellite connectivity enabled monitoring of data quality and Geode ‘health’ to ensure a successful survey.

To obtain a 3D model of subsurface shear-wave velocities, a fully probabilistic 2-step tomography workflow is used. Throughout the workflow a pre-computed library of velocity depth profiles along with their associated dispersion curves and sensitivity kernels (Geolibrary; Fig. 4, Table 1) is used for fitting and training tasks. Phase velocity dispersion measurements are initially extracted from the cross-correlation functions (CCF) for each Geode pair. This is done by fitting the real part of the Fourier transform of the correlation functions with a zero-order Bessel function of the first kind (Aki, 1957; Ekström et al., 2009) using a weighted hierarchical L2-norm based minimisation approach to recover the pairwise dispersion probability density. The first step of the modelling workflow uses the extracted pairwise measurements to invert for the 2D probability density of phase velocity at each frequency. This is achieved through ensemble inference, which employs a data-adaptive Voronoi parameterization and Markov Chain Monte Carlo (MCMC) sampling. The second step of the workflow inverts for the probability density of shear-velocity vs. depth for every x,y column of the model parameter space using a deep neural network (DNN) pre-trained using the Geolibrary to perform a mapping from Rayleigh wave dispersion curve to velocity depth profile in a much more efficient manner than conventional Monte Carlo-based methods. This integrated approach facilitates the rapid construction of robust 3D models, leveraging uncertainties from earlier stages to enhance the accuracy of the final model and quantify its uncertainty. The model output has been clipped to the tenement boundaries of Inflection

Resources, however, in principle the model extends to the entire area within which raypaths are measured.

Gravity inversion modelling

The airborne gravity data utilised in this study was sourced from the publicly accessible Geological Survey of New South Wales (NSW) database. This dataset was collected by Xcalibur Smart Mapping (XSM) as part of the NSW Live Program, which spanned from mid-2022 to mid-2023. The survey was conducted at a spacing of 2 km, providing detailed coverage of the region. The Bouguer gravity data was derived by applying a terrain correction, using a standard crustal density of 2.67 g/cc. After first reprojecting the data from WGS 84 UTM Zone 54S to WGS 84 UTM Zone 55S, the reference frame for our ANT survey, the regional and residual gravity components were separated using a filtering technique to isolate long-wavelength signals, representing the regional field, from short-wavelength signals, representing the residual field (Uieda et al., 2020). The residual gravity anomaly was then derived by subtracting the regional field from the observed gravity data in order to ensure the model reflects the near-surface elements of the gravity field rather than longer wavelength influence of the regional field.

The inversion of the residual gravity data was conducted to generate a 3D subsurface density distribution model. For this purpose, we utilised SimPEG (Simulation and Parameter Estimation in Geophysics), an open-source library designed for solving inverse problems in geophysics (Cockett et al., 2015). The inversion process begins with the definition of a subsurface model, typically represented as a discretized grid or mesh. The grid was defined with a resolution of 500 m in the x and y directions and 250 m in the z direction, to a maximum depth of 4.5km, encompassing the study area in three dimensions.

Each grid cell was assigned an initial density value. The inversion process iteratively adjusts these initial density values to minimise the difference between the observed gravity anomalies (residual data) and the gravity response predicted by the model. To ensure that the resulting model is geologically plausible, regularisation techniques were applied. In this study, we employed Tikhonov regularisation, which strikes a balance between fitting the data and maintaining the smoothness of the model through a cooling beta approach (Cockett et al., 2015). SimPEG uses a gradient-based Gauss–Newton optimization algorithm to iteratively refine the model parameters. Starting from an initial guess, the algorithm computes the predicted gravity response and compares it to the observed residual data. The resulting misfit is used to update the model, reducing the misfit in subsequent iterations. This iterative process continues until convergence is achieved, indicating that the model adequately explains the observed data within an acceptable tolerance. The final output of the inversion is a 3D model of the subsurface density distribution, revealing spatial variations in density that provide valuable insights into the geological structure of the study area.

Results: ANT data quality

Cross-correlation beamforming analysis of the recorded ambient seismic noise, based on the seismic wave arrival times correlated between sensor pairs and the geometry of the sensor network (Ruigrok et al., 2017), reveals primary seismic noise sources predominantly located towards the northwest and southeast directions (Fig. 5a, b, c). This directional alignment is advantageous for long- and mid-distance receiver (Geode) pairs. The observed azimuth aligns with the locations of regional population centres, including Bourke to the northwest, Cobar to the west, and Dubbo, Parks, and Orange to the southeast. The regional survey successfully recovered surface wave signals within the 0.2 - 1.2 Hz frequency range. Although the beamforming results show a moderately directional distribution of sources, the low normalised beam power values indicate that no single ambient noise source significantly dominates the wavefield. This lack of dominance is an important assumption for the validity of the retrieved velocity measurements. Figure 5d presents a bandpass filtered cross-correlation moveout plot, which shows a high-quality fundamental mode surface wave signal. This signal returns an average signal-to-noise ratio (SNR) of approximately 6 across the full range of Geode pair separation, indicating a moderate signal strength, and shows clear dispersive characteristics. Figure 5e displays the frequency-wavenumber (FK) spectrum derived from the cross-correlated data and illustrates the relationship between frequency and apparent velocity in the signal, providing insight into the wave propagation characteristics across different frequencies. Figure 6 shows the convergence to a stable SnR after approximately 12 days, which sets a benchmark for district-scale ANT survey operations in the Macquarie Arc. Real-time updates of survey data, cross-correlation SnR and Geode health are received every 6 hours during survey operations, which enables adaptation of deployment operations in the field to a predictable schedule which optimises for data coverage over time, yet remains adaptable to seismic and environmental conditions. Overall, the data retrieved during the survey is of a high quality and insights across the frequency range provide a solid foundation from which to develop a 3D velocity model.

Results: ANT velocity model

The ANT velocity model has a cell size of 250m and the resolution of the model is on the order of 1km, given the Geode spacing. Features smaller than this will be unlikely to be imaged. The model demonstrates velocities up to a maximum ~3900m/s and a minimum ~2500m/s (Fig. 7a). As the abundance of cross-correlated ray paths are a measure of confidence, the most well-resolved portions of the model are where there are greater ray paths, leading to an overall confidence index that shows the central portions of the model are better resolved (Fig. 7b). Features outside the highly confident regions will be poorly resolved, however, the geometry of the array means that the high confidence regions lie within the survey bounds. Some cross-correlated rap paths do extend across areas adjacent to the core of the survey, however, these areas are not considered in terms of our description and analysis of the various velocity features.

As seismic velocity increases with depth due to increased compaction by overburden, the model shows an expected increase in velocity with depth (Fig. 8). There is also considerable variation in velocity along strike (Fig. 8). The most significant elements of the model are the presence of a northwest trending discontinuity running parallel to the long axis of the survey as indicated by the dashed line at the various depth slices in Figure 8; and the distinct seismic velocity profiles between the northwestern and southeastern areas.

This northwestern area shows several key features (see cross section Fig. 9a) including:

- a relatively low velocity uppermost layer with velocity averaging ~2500m/s down to depths of around 400m (V1);
- a zone of intermediate velocity, ~3000 - 3100 m/s, with a lenticular shape extending down to ~2200m (V2), and with an apparently lower velocity zone beneath; and
- a high velocity zone at the base of the model averaging ~3600m/s (V3) and with a zone of markedly lower velocity in the centre of this high velocity zone (V4) in which the lowermost part of the model images velocities of ~3300 - 3400m/s. Notably, this relatively lower velocity central portion lies beneath the larger of the two elliptical intermediate velocity zones (V2).

In the southern area of the survey, the model shows some similarities with the northern area, including the presence of a low velocity upper zone, intermediate velocity middle zone and a high velocity lower zone, however, there are several differences to the geometry of these layers (Fig. 9b) including:

- the uppermost 500m of the model, which has a low velocity (<2500m/s) layer only in the western edge of the survey (V5) that extends down to a depth of ~1600m where this low velocity zone transitions to a zone of relatively high velocity, ~3500m/s (V6). Note, however, that the velocities in this lowermost western portion of the model (V6) are lower than in the lower 2km to the east (V7) where velocity reaches up to ~3850m/s or more. This west-east transition is concentrated in the immediate vicinity of the western edge of the mode.
- The intermediate velocity zone in the upper 2000m of the model is, in this southern area, a significant elliptical body of intermediate velocity (V7, ~3300m/s).
- The easternmost upper portion of the model (V8) shows lower velocities than in the centre of the intermediate velocity body (V7), down to 3000m/s.
- The lower portion of the model shows fairly homogenous velocities to ~3900 m/s (V9).

Results: gravity inversion modelling

Within the study area, the Bouguer anomaly map reveals both low and high-frequency anomalies, indicating the presence of large-scale, deep-seated structures as well as masses in the shallow crust, with amplitude variations ranging from -25 to 23.4 mGal. The gravity inverse model, which is built on the residual gravity, emphasises the prominent ridge of high gravity

that runs through the study area in a northwest orientation (Fig. 10). This central gravity ridge has two zones in which the gravity response is distinctly lower; in the northwest, coincident with a series of interpreted intrusive complexes (G1), and in the southern area, coincident with the magnetically quiet zone of the Silurian basin (G2; Fig. 10). Within this northern zone of lower gravity (G1), there is a prominent high density body extending from depth upwards and is visible in the 2.69 g/cc and 2.71 g/cc isosurfaces (G3). Note that there is a prominent ~5km wide zone of high gravity extending towards the northwest (G4) towards the northern low gravity zone that encompasses G1 and G3 that has an apparent southwest dip (Fig. 10). The eastern half of the gravity model is dominated by rocks with low gravity response, with a series of smaller, higher gravity bodies occurring in the uppermost portion of the model (e.g. G5). These gravity bodies are modelled as having limited depth and are prominent in the 2.67 g/cc isosurface.

Discussion

The new ANT velocity model provides a view of the subsurface across an area of some 1,800 km2 and is sensitive to features of the geology that have a scale in the order of >1km. We discuss the key features of the velocity model with reference to the potential field geophysics and available drilling across the region. Considering the features in the ANT velocity model with respect to the gravity inversion, we then provide a discussion of the value of ANT in district-scale studies in the context of a mineral systems understanding of the region, and exploration for magmatic hydrothermal deposits more broadly.

It is worth pointing out that it may be possible to jointly invert the surface wave dispersion measurements with the Bouguer gravity data (Maceira and Ammon, 2009). However, this procedure requires an empirical relationship between seismic velocity and density, such as Brocher's relationship (Brocher, 2005). A comprehensive empirical relationship between seismic velocity and density for the Macquarie Arc has not been compiled, but could be investigated in future work with petrophysical measurements.

In addition, we note that although the entire survey region lies beneath approximately 100 to 400m of Mesozoic and Cenozoic cover, the model does not resolve the variation in cover thickness well. To better resolve cover units at this scale a survey with smaller site spacing would be required, with spacing on the order of the expected cover thickness, since the high frequency seismic energy that is required to image the shallow subsurface is attenuated before reaching neighbouring stations.

ANT velocity model and relationship to gravity inversion

Many of the major features of the ANT velocity model can be related to the potential field data, from which an interpretation of the subsurface geology can be made. The first order structural

feature of the area is the northwest-trending magnetic and gravity velocity discontinuity, which defines a major shear zone. In both the velocity model and the gravity model this shear zone appears to be steeply south-westerly dipping (Fig. 11).

One of the most intriguing aspects of the ANT velocity model is the presence of ovoid shaped velocity bodies in the upper 3km. In the northern region of the model, in the vicinity of the velocity zones labelled V2 and gravity zones labelled G1 and G3, there are several features like this that extend upwards and outwards from deeper levels of the model (Fig. 12). These velocity features are most obvious in the shape of the isosurfaces with values 3050 m/s and 3100 m/s (Figs. 11, 12a). In addition, the velocity feature V2 of the plutonic bodies appears to be connected to a velocity second feature that is slightly deeper and offset towards the northwest labelled feature V2a in Figure 13b. Intriguingly, these velocity features are found in regions where there is a corresponding gravity low feature (G1); thus, when compared to the gravity isosurface at 2.70 g/cc, the velocity features are antithetic to the location of several gravity high zones with pipe-like geometry that extend from near the surface down towards the base of the model (Fig. 13). Importantly, these velocity features correlate with textures in the magnetic intensity images that appear to be magmatic bodies.

One interpretation of these features is that the intermediate velocity body highlights the presence of a pluton with a laccolith-type geometry. The antithetic relationship between this intermediate velocity and gravity >2.70 g/cc suggests that if this is a pluton, it is likely not mafic in composition, since gabbro for example typically has higher densities (e.g. Shin et al., 2021; Zappone and Kissling, 2021) and is possibly therefore felsic or intermediate in composition. The gravity values >2.70 g/cc adjacent to these velocity features is likely to represent zones in which the bulk lithology is dominated by mafic to intermediate volcanic rocks of the Macquarie Arc into which the felsic or intermediate composition plutons were emplaced.

In the southern portion of the survey area there is a second example of an intermediate velocity body (V8) that corresponds to a magnetic feature that is consistent with there being a pluton in this region (Fig. 14). To the east of the velocity body however, the velocity is lower at the same depth as the velocity body (V8). There is nothing in the magnetic intensity images to suggest that the plutonic bodies in this area would necessarily be at different depths; both appear to have similar clarity in the magnetic images which is unlikely if one was significantly deeper than the other (Fig. 14). It is possible that the high velocity feature does not directly correlate with the magnetic features. In addition, the gravity model in this area suggests that it is unlikely that a deeper highly dense body such as a gabbro or mafic-rich cumulate body underlying these plutons. Therefore, it may be that the high velocity body is imaging a deeper, more structurally coherent portion of a predominantly felsic intrusive body. A greater degree of deformation within the eastern pluton may cause it to have relatively lower velocity than the intermediate velocity body (V8). This could be because the V8 body is more competent that has suffered less deformation, or be a younger body that has intruded into pre-existing pluton(s).

Significance of district-scale ANT surveys for scale reduction

In magmatic hydrothermal systems such as porphyry copper-gold deposits kilometre-scale plutons are the source regions for the narrow, steeply dipping porphyry intrusions (e.g. Heinrich, 2024). These plutons represent upper crustal magma chambers that did not erupt, causing in situ crystallisation of the magma, leading to fractionation of the remaining melt and concentration of incompatible metals into late stage fluids. The overpressure of these fluids and remaining magma leads to breakouts from the magma chambers, facilitated by seismic events and injection of subsequent batches of magma from deeper feeder zones. These breakouts become the porphyry intrusions that are the targets for mineral exploration.

With this in mind, the plutons imaged in the district scale ANT at the velocity features V1 and V8 are a compelling result. The extent of these zones of relatively high velocity is likely an indicator of the size of the plutonic body. In addition, the ANT provides an image of a possible upper crustal magma plumbing system at the velocity feature V2, with the second, deeper feature V2a being a possible feeder zone for the shallower pluton at velocity feature V2. Since most metallogenically fertile batholiths are complex and multiphase, the presence of possible feeder zones connecting deeper and shallower bodies may be significant and zones such as this are of exploration interest.

Furthermore, the seismic images of these interpreted plutonic bodies reveal they are connected spatially with the ridge of velocity that corresponds to the main shear zone in the area. This is an interesting result and may suggest that this shear zone has provided a zone of weakness along which magmas have been directed towards the upper crust. Nevertheless, the shear zone dissects the major igneous bodies seen in the magnetic intensity images. This suggests that this is a long lived zone of structural weakness that may have extended at least from the time of emplacement of the plutonic bodies (Ordovidian to Silurian) during which it facilitating magma flow, through to subsequent reactivation during the final phases of deformation in the region, likely after Devonian basin formation, deposition and magmatism (e.g. Tabberabberan event).

When combined with the gravity inversion, we now have a new view of the density profile of the upper crust. The presence of low gravity domains that correspond to magmatic-textured magnetic domains and intermediate velocity bodies is a very useful indicator that these subsurface features are broadly felsic in composition as opposed to high density mafic rocks. Importantly, with the addition of seismic velocity information there is now a direct image of the depth of the feature in question. Infill ANT surveys at a smaller scale, for example Geode spacing of <500 m, can image key geological features. Such smaller scale surveys can be designed to identify velocity structures associated with intrusive stocks and their alteration zones.

This study shows that district-scale ANT has a potentially significant role in helping to visualise magmatic plumbing systems of granitic complexes, and can therefore be utilised as part of a systematic process of scale reduction in a covered, greenfields exploration program. The ANT velocity model also provides insight into the fundamental geological architecture of the region,

which is helpful for studies of crustal evolution. An area for further research is to understand what are the causes of the seismic velocity variations that can be imaged using ANT. Here, we have taken the approach that the velocity is largely a reflection of variations in composition and hence density. However, we note that there are other regions within the model that have clear igneous intrusive textures in the magnetic data, but they have not been significantly imaged in the velocity model. Most likely, this indicates there is not sufficient velocity contrast between the igneous bodies in question and their host rocks for them to be clearly defined in the velocity model.

It is important for mineral explorers to note that the district-scale of the survey presented here necessarily results in an 'averaging' effect to the subsurface velocity properties. Small features will not be detected. Further, like all geophysical methods, ANT relies on contrasting physical properties between the subsurface rock units for those rocks to be imaged. It may be that at the scale of this district-scale survey, there is not sufficient contrast between some of the intrusions and the host rocks. However, if a survey were to be conducted at a smaller scale the granularity of the velocity image will be improved. Finally, it is necessary to consider all geological information when identifying prospective areas during the scale-reduction process.

Conclusion

In this study we have applied wide-spaced (~5 km) seismic sensors and ambient noise tomography to image to depths of ~5 km across a region of over area of 1,800km2, which lies buried beneath a veneer of younger sedimentary cover. The broad patterns of the resulting ANT velocity model are consistent with the known geology and potential field data which suggest the presence of intrusive bodies within volcanic and volcaniclastic rocks of the Macquarie Arc and adjacent Siluro-Devonian basins.

Important features of the model are ovoid, intermediate velocity zones in the upper 2 km of the model, which correspond to igneous textured bodies in magnetic data. These bodies are spatially associated with low gravity domains in the inversion model of the regional gravity data. This indicates that the new ANT velocity model is likely imaging plutonic bodies in the uppermost crust and that these bodies are connected both to each other, and to a major structure that dissects the survey area.

In terms of magmatic-related mineral systems, detecting the presence of sizeable intrusive bodies is of interest since porphyry-epithermal systems typically develop above kilometre-scale plutonic bodies (Heinrich, 2024). These bodies are therefore areas of interest for follow up geophysical or geological investigations. The capacity to image the geometry of kilometre-scale igneous bodies is a significant outcome of this ANT survey and provides an example of scale-reduction by undertaking a large-scale survey early on in the process of mineral exploration to highlight areas of interest.

Acknowledgements

Fleet Space Technologies operations team, especially Robyn Clay and Jason Hodge, are acknowledged for their work in delivering the ANT deployment reported on here, as is CEO Flavia Tata Nardini for support to publish. Karen Conors provided very helpful comments on an earlier version.

Source of funding

Funding for this study was provided by Fleet Space Technologies.

Disclosure statement

The authors report there are no competing interests to declare.

ORCID

Anthony Reid: https://orcid.org/0000-0002-9435-9342
Gerrit Olivier: https://orcid.org/0000-0002-2083-5895

Data availability

Data arising from this study is available upon request to Fleet Space Technologies.

References

Aki, K. 1957. Space and time spectra of stationary waves with special reference to microtremors. Bulletin Earthquake Research Institute University of Tokyo 35, 415–456.

Bensen, G.D., Ritzwoller, M.H., Barmin, M.P., Levshin, A.L., Lin, F., Moschetti, M.P., Shapiro, N.M., and Yang, Y. 2007. Processing seismic ambient noise data to obtain reliable broad-band surface wave dispersion measurements. Geophysical Journal International 169, 1239–1260.

Brocher, T.M. 2005. Empirical relations between elastic wavespeeds and density in the Earth's crust. Bulletin of the Seismological Society of America 95, 2081–2092.

Chalmers, D.I., Ransted, T.W., Kairaitis, R.A., and Meates, D.G. 2007. The Wyoming gold deposits: volcanic-hosted lode-type gold mineralisation in the eastern Lachlan Orogen, Australia. Mineralium Deposita 42, 505–513.

Clowes, R.M., Hammer, P.T.C., Fernández-Viejo, G., and Kim Welford, J. 2005. Lithospheric structure in northwestern Canada from Lithoprobe seismic refraction and related studies: a synthesis,. Canadian Journal of Earth Sciences 42, 1277–1293.

Cockett, R., Kang, S., Heagy, L.J., Pidlisecky, A., and Oldenburg, D.W. 2015. SimPEG: An open source framework for simulation and gradient based parameter estimation in geophysical applications. Computers & Geosciences 85, 142–154.

Cooke, D.R., Wilson, A.J., House, M.J., Wolfe, R.C., Walshe, J.L., Lickfold, V., and Crawford, A.J. 2007. Alkalic porphyry Au – Cu and associated mineral deposits of the Ordovician to Early Silurian Macquarie Arc, New South Wales. Australian Journal of Earth Sciences 54, 445–463.

Crawford, A.J., Cooke, D.R., and Fanning, C.M. 2007a. Geochemistry and age of magmatic rocks in the unexposed Narromine, Cowal and Fairholme Igneous Complexes in the Ordovician Macquarie Arc, New South Wales. Australian Journal of Earth Sciences 54, 243–271.

Crawford, A.J., Glen, R.A., Cooke, D.R., and Percival Guest Editors, I.G. 2007b. Geological evolution and metallogenesis of the Ordovician Macquarie Arc, Lachlan Orogen, New South Wales. Australian Journal of Earth Sciences 54, 137–141.

Dwyer, R., Forster, D.B., Simpson, B., Blevin, P.L., and Huang, H. 2025. Relationships between high-K magmas and Cu-Au porphyry deposits in the Macquarie Arc, Australia. Geological Society, London, Special Publications 551.

Ekström, G., Abers, G.A., and Webb, S.C. 2009. Determination of surface‐wave phase velocities across. Geophysical Research Letters 36, L18301.

Fergusson, C.L. 2009. Tectonic evolution of the Ordovician Macquarie Arc, central New South Wales: arguments for subduction polarity and anticlockwise rotation. Australian Journal of Earth Sciences 56, 179–193.

Fitzpatrick, N.J. 2005. Second Annual Report on EL6345, Canonba Project, covering period 19 November 2006 to 18 November 2006 (Mining Exploration and Geoscience Division, Government of New South Wales).

Glen, R.A., Crawford, A.J., and Cooke, D.R. 2007. Tectonic setting of porphyry Cu – Au mineralisation in the Ordovician – Early Silurian Macquarie Arc, Eastern Lachlan Orogen, New South Wales. Australian Journal of Earth Sciences 54, 465–479.

Glen, R.A., Quinn, C.D., and Cooke, D.R. 2012. The Macquarie Arc, Lachlan Orogen, New South Wales: its evolution, tectonic setting and mineral deposits. Episodes 35, 177–186.

Glen, R.A., Saeed, A., Quinn, C.D., and Griffin, W.L. 2011. U–Pb and Hf isotope data from zircons in the Macquarie Arc, Lachlan Orogen: Implications for arc evolution and Ordovician palaeogeography along part of the east Gondwana margin. Gondwana Research 19, 670–685.

Glen, R., Crawford, A., and Cooke, D. 2003. Tectonic setting of porphyry copper-gold mineralisation in the Macquarie arc. In Magmas to Mineralisation: The Ishihara Symposium. Blevin, B. Chappell, and M. Jones, eds. (Canberra: Geoscience Australia, Commonwealth of Australia), pp. 65–68.

Groome, M., Tosdal, R.M., Harris, A.C., and Percival, I.G. 2021. Preservation of the Cadia Valley porphyry Au–Cu district, NSW, Australia: Silurian basin formation and subsequent inversion. Australian Journal of Earth Sciences 68, 799–817.

Groves, D.I., Santosh, M., Müller, D., Zhang, L., Deng, J., Yang, L.-Q., and Wang, Q.-F. 2022. Mineral systems: Their advantages in terms of developing holistic genetic models and for target generation in global mineral exploration. Geosystems and Geoenvironment 1, 100001.

Hammer, P.T.C., Clowes, R.M., Cook, F.A., van der Velden, A.J., and Vasudevan, K. 2010. The Lithoprobe trans-continental lithospheric cross sections: imaging the internal structure of the North American continent. Canadian Journal of Earth Sciences 47, 821–857.

Heinrich, C.A. 2024. The chain of processes forming porphyry copper deposits.Economic Geology 119, 741–769.

Heinson, G., Didana, Y., Soeffky, P., Thiel, S., and Wise, T. 2018. The crustal geophysical signature of a world-class magmatic mineral system. Scientific Reports 8, 10608.

Hoggard, M.J., Czarnota, K., Richards, F.D., Huston, D.L., Jaques, A.L., and Ghelichkhan, S. 2020. Global distribution of sediment-hosted metals controlled by craton edge stability. Nature Geoscience 13, 504–510.

Holliday, J.R., Wilson, A.J., Blevin, P.L., Tedder, I.J., Dunham, P.D., and Pfitzner, M. 2002. Porphyry gold–copper mineralisation in the Cadia district, eastern Lachlan Fold Belt, New South Wales, and its relationship to shoshonitic magmatism. Mineralium Deposita 37, 100–116.

Hughes, W.S. 1998. First annual exploration report, EL 5177, Narromine area (Mining Exploration and Geoscience Division, Government of New South Wales).

Jones, T., Olivier, G., Murphy, B., Cole, L., Went, C., Olsen, S., Smith, N., Gal, M., North, B., and Burrows, D. 2024. Real-Time Ambient Seismic Noise Tomography of the Hillside Iron Oxide–Copper–Gold Deposit. Minerals 14, 254.

Kirkby, A.L., Musgrave, R.J., Czarnota, K., Doublier, M.P., Duan, J., Cayley, R.A., and Kyi, D. 2020. Lithospheric architecture of a Phanerozoic orogen from magnetotellurics: AusLAMP in the Tasmanides, southeast Australia. Tectonophysics 793, 228560.

Kreuzer, O.P., Miller, A.V.M., Peters, K.J., Payne, C., Wildman, C., Partington, G.A., Puccioni, E., McMahon, M.E., and Etheridge, M.A. 2015. Comparing prospectivity modelling results and past exploration data: A case study of porphyry Cu–Au mineral systems in the Macquarie Arc, Lachlan Fold Belt, New South Wales. Ore Geology Reviews 71, 516–544.

Maceira, M., and Ammon, C.J. 2009. Joint inversion of surface wave velocity and gravity observations and its application to central Asian basins shear velocity structure. Journal of Geophysical Research: Solid Earth 114, 10.1029/2007JB005157.

Menzies, D., Marris, K., Erskine, T., and Waddell, A. 2024. Exploring for alkalic porphyry-related Cu-Au mineralisation in the northern Junee-Narromine Macquarie Arc; a focus on Myallmundi and Duck Creek projects. In Bulletin 76: Discoveries in Tasmanides 2024, J.E. Greenfield, ed., Australian Institute of Geoscientists, pp. 172–184.

O'Donnell, J.P., Agrawal, S., Eakin, C.M., Thiel, S., Brand, K., Gorbatov, A., and Goleby, B. 2023. Mapping crustal structure across southern Australia using seismic ambient noise tomography. Gondwana Research 121, 307–324.

Olivier, G., Borg, B., Trevor, L., Combeau, B., Dales, P., Gordon, J., Chaurasia, H., and Pearson, M. 2022. Fleet's Geode: A Breakthrough Sensor for Real-Time Ambient Seismic Noise Tomography over DtS-IoT. Sensors 22, 8372.

Rawlinson, N., Davies, D.R., and Pilia, S. 2017. The mechanisms underpinning Cenozoic intraplate volcanism in eastern Australia: Insights from seismic tomography and geodynamic modeling. Geophysical Research Letters 44, 9681–9690.

Ruigrok, E., Gibbons, S., and Wapenaar, K. 2017. Cross-correlation beamforming. Journal of Seismology 21, 495–508.

Sanchez, G., Stewart, A.J., Liu, S., Highet, L.M., Woods, M., Brown, C.M., Bonnardot, M.-A., Beyer, E.E., Clark, A., Connors, K., et al. 2024. Layered Geology of Australia, 1:1 000 000 scale (Canberra: Geoscience Australia, Commonwealth of Australia).

Shapiro, N.M., Campillo, M., Stehly, L., and Ritzwoller, M.H. 2005. High-resolution surface-wave tomography from ambient seismic noise. Science 307, 1615–1618.

Sherwin, L. 1996. Narromine 1:250 000 Geological Sheet SI/55-3: Explanatory Notes (Geological Survey of New South Wales).

Shin, S., Cho, S., Kim, E., and Lee, J. 2021. Geophysical properties of Precambrian igneous rocks in the Gwanin vanadiferous titanomagnetite deposit, Korea. Minerals (Basel, Switzerland) 11, 1031.

Squire, R.J., Herrmann, W., Pape, D., and Chalmers, D.I. 2007. Evolution of the Peak Hill high-sulfidation epithermal Au–Cu deposit, eastern Australia. Mineralium Deposita 42, 489–503.

Uieda, L., Soler, S.R., Pesce, A., Oliveira, V.C., Jr, and Shea, N. 2020. Harmonica: Forward modeling, inversion, and processing gravity and magnetic data. https://zenodo.org/records/3628742.

Watkins, J.K., and Meakin, N.S. 1996. Nyngan and Walgett 1:250 000 Geological Sheets SH/55-15 & SH/55-11: Explanatory Notes (Sydney: Geological Survey of New South Wales).

Zappone, A., and Kissling, E. 2021. SAPHYR: Swiss Atlas of Physical Properties of Rocks: the continental crust in a database. Swiss Journal of Geosciences 114, 13.

Figures

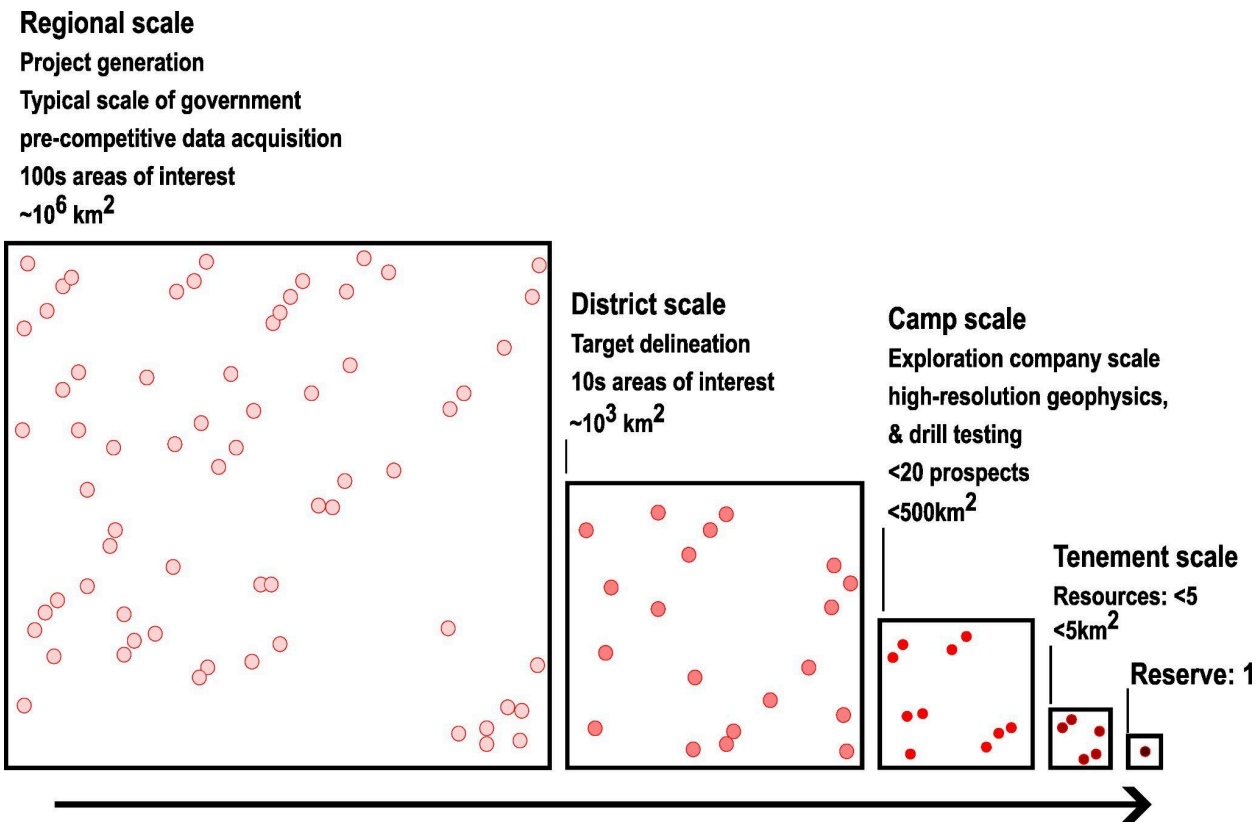

Figure 1. Conceptual diagram of the progression from regional to tenement scale area reduction in mineral exploration. Red circles suggest areas of interest at each scale. From many areas of interest at the larger scale progressively smaller areas are focussed on in order to ideally discover economic mineral resources and reserves at the tenement scale. This work particularly addresses the scale between regional scale and camp scale, typically conducted by precompetitive government surveys and mineral exploration companies respectively. This graphic has been adapted from a similar diagram by Evolution Mining, https://evolutionmining.com.au/the-exploration-process.

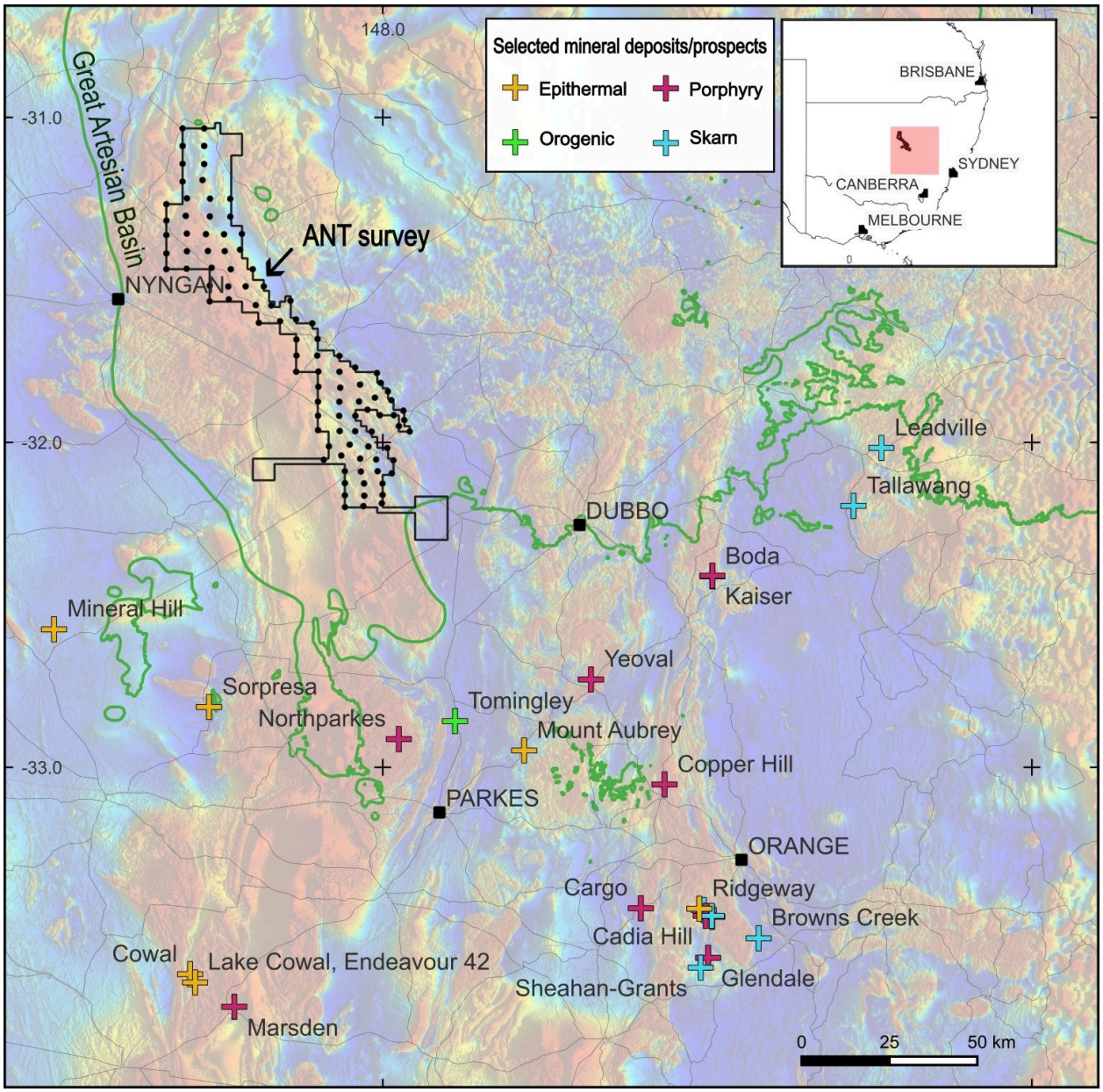

Figure 2. Location of district scale ANT survey, central New South Wales with total magnetic intensity image. ANT survey was undertaken using Fleet Space Technologies proprietary seismometers, Geodes, across a contiguous tenement package of Inflection Resources. The location of the known mineral deposits is strongly correlated with the absence of Mesozoic, Great Artesian Basin sediments. The southern extent of the Mesozoic sediment is shown in outline. Geophysical image, geological outline and locations of mineral deposits/prospects from Geological Survey of New South Wales, MinView, https://minview.geoscience.nsw.gov.au/

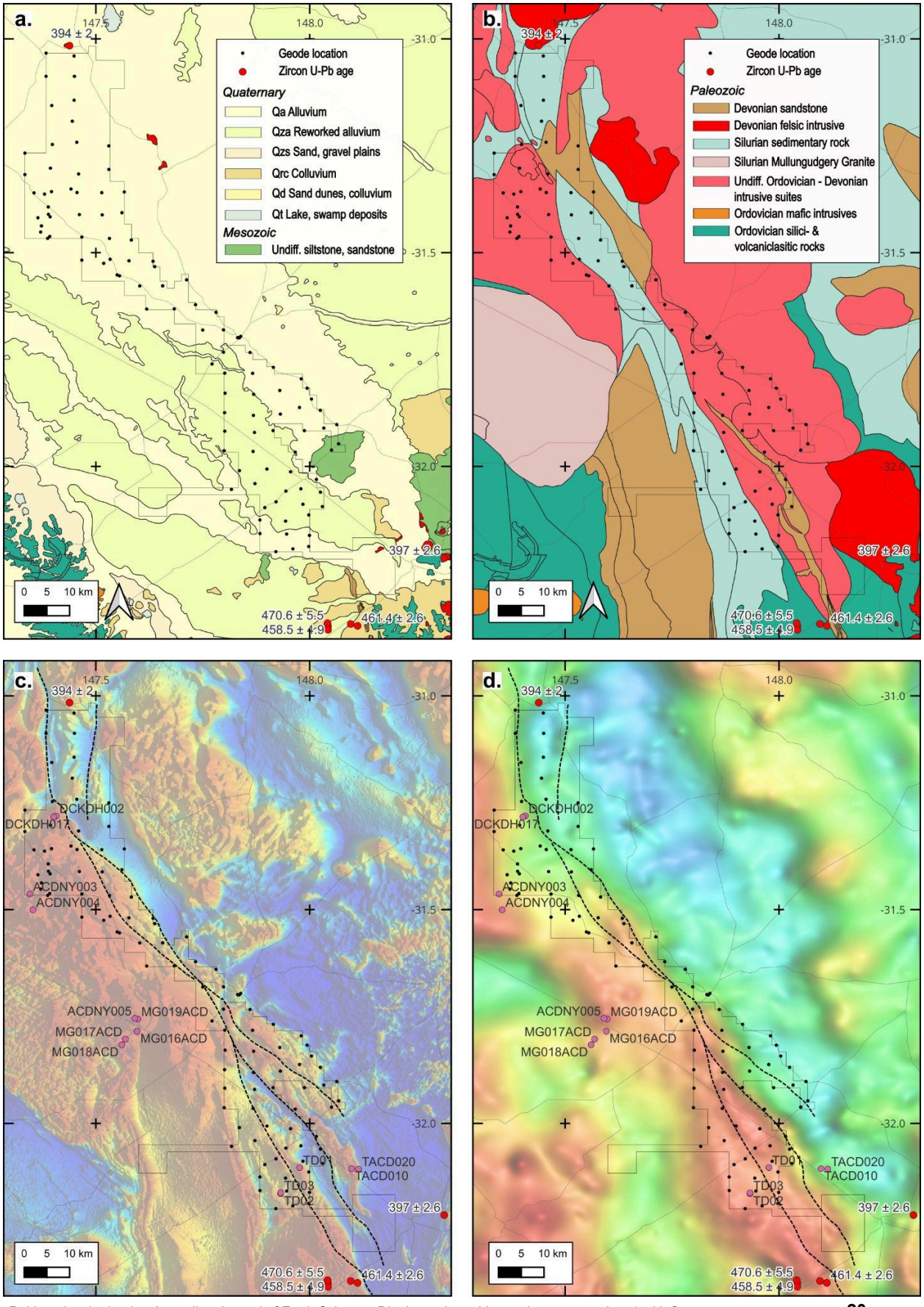
a.
b.
c.
d.
147.5
148.0
-31.0
-31.5
-32.0
394 ± 2
397 ± 2.6
470.6 ± 5.5
458.5 ± 4.9
461.4 ± 2.6
0 5 10 km
Geode location
Zircon U-Pb age
Quaternary
Qa Alluvium
Qza Reworked alluvium
Qzs Sand, gravel plains
Qrc Colluvium
Qd Sand dunes, colluvium
Qt Lake, swamp deposits
Mesozoic
Undiff. siltstone, sandstone
Paleozoic
Devonian sandstone
Devonian felsic intrusive
Silurian sedimentary rock
Silurian Mullungudgery Granite
Undiff. Ordovician - Devonian intrusive suites
Ordovician mafic intrusives
Ordovician silici- & volcaniclasitic rocks
DCKDH002
DCKDH017
ACDNY003
ACDNY004
ACDNY005
MG019ACD
MG017ACD
MG016ACD
MG018ACD
TD01
TACD020
TACD010
TD03
TD02

Figure 3. Geological and potential field data across the survey area, highlighting the location of ANT stations (black circles) in the context of the relevant contiguous tenements of Inflection Resources, and publicly available drill holes (purple circles) and U-Pb zircon geochronology (red pentagon). Ages are listed as age, error and given in Ma. The location of the major shear zones that cut through the survey area (dashed line) is indicated on the potential field images. Surface geology and Paleozoic interpreted geology information from Layered Geology of Australia 1:1,000,000 scale 2024 Edition, Geoscience Australia (Sanchez et al., 2024), Other geological and geophysical data from Geological Survey of New South Wales, MinView https://minview.geoscience.nsw.gov.au/. **a.** Surface geology map of survey area. **b.** Interpreted Paleozoic basement geology. **c.** Reduced to pole, total magnetic intensity image. **d.** Isostatic Bouger gravity image.

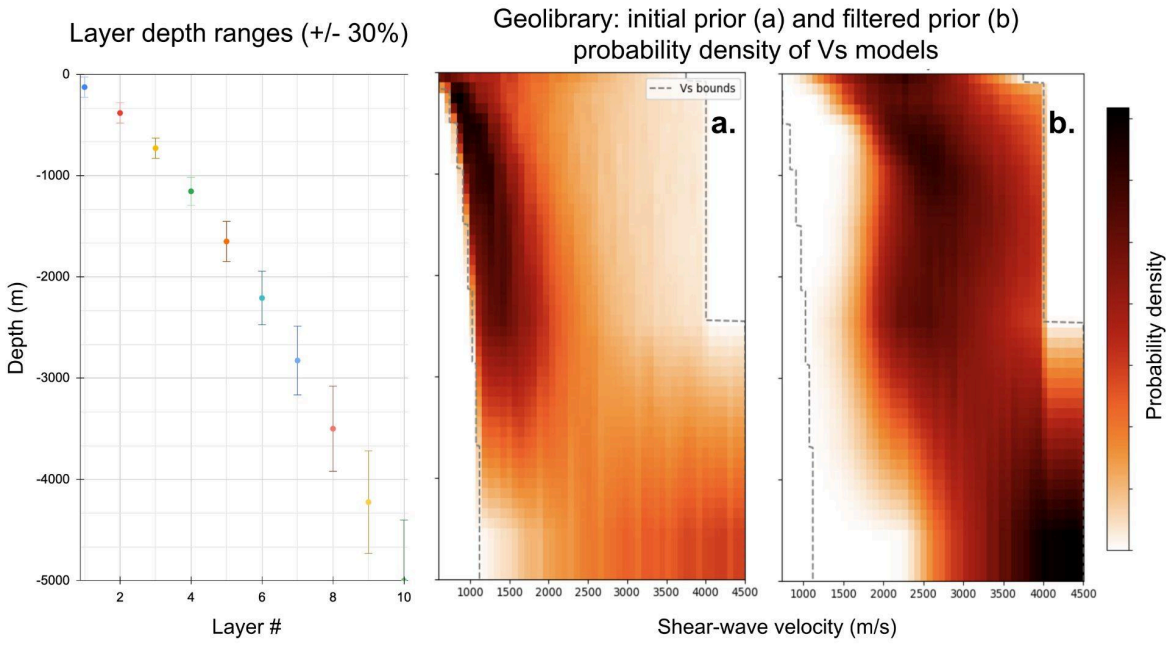

Figure 4. Summary of the Vs - depth model parameterisation for the pre-computed library of velocity models (Geolibrary) developed for the Junee-Narromine district survey, showing layer depth ranges (left) and prior and filtered probability density of the models (right). Geolibrary filtering is performed in phase velocity - frequency space based on the estimated array average dispersion +/- 1000m/s.

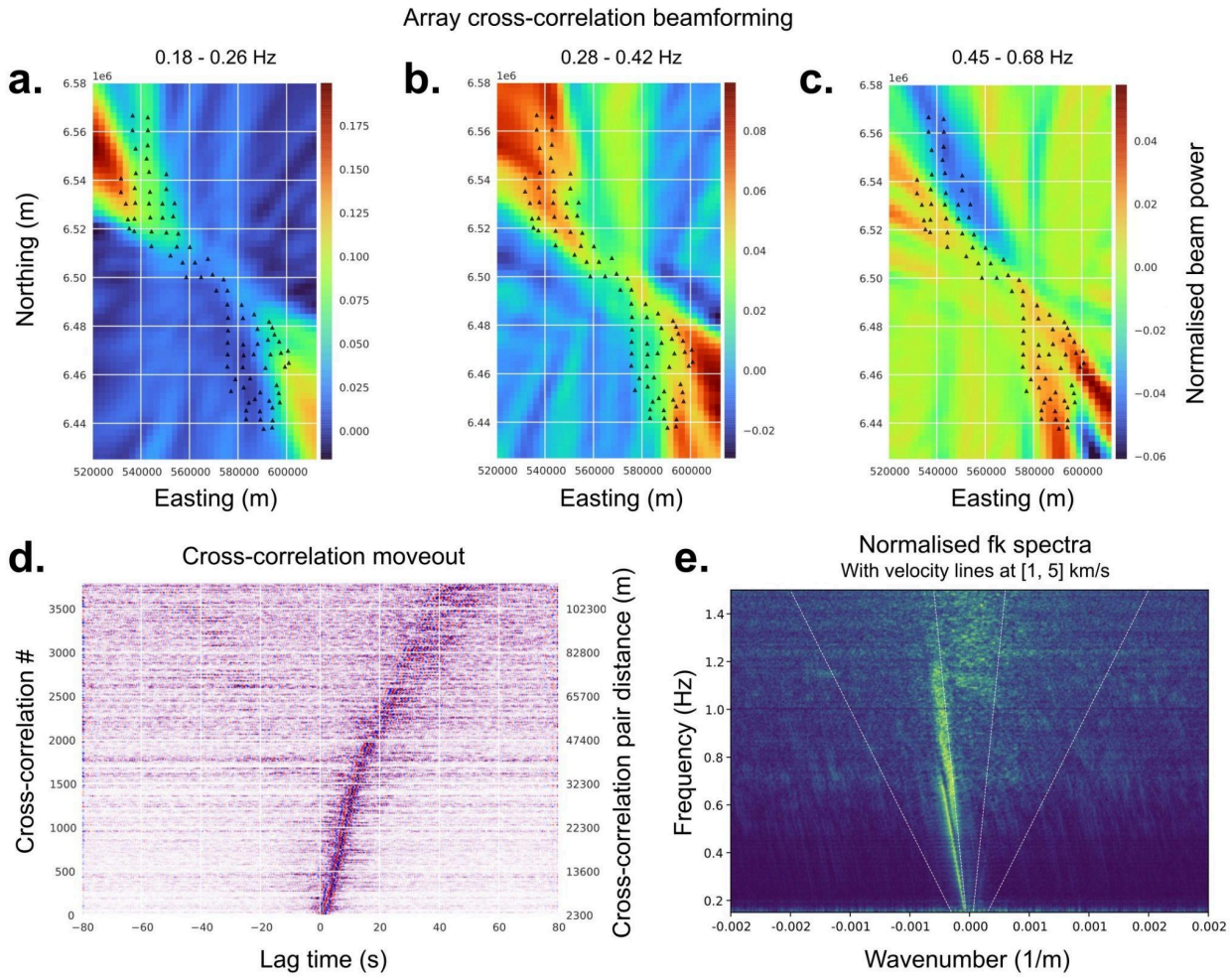

Figure 5. ANT seismic data quality indicators. **a.** Beamforming plot for 0.18 - 0.26 Hz. **b.** Beamforming plot for 0.28 - 0.42 Hz. **c.** Beamforming plot for 0.45 - 0.68 Hz. **d.** Cross-correlation moveout plot. **e.** Normalised F-K plot.

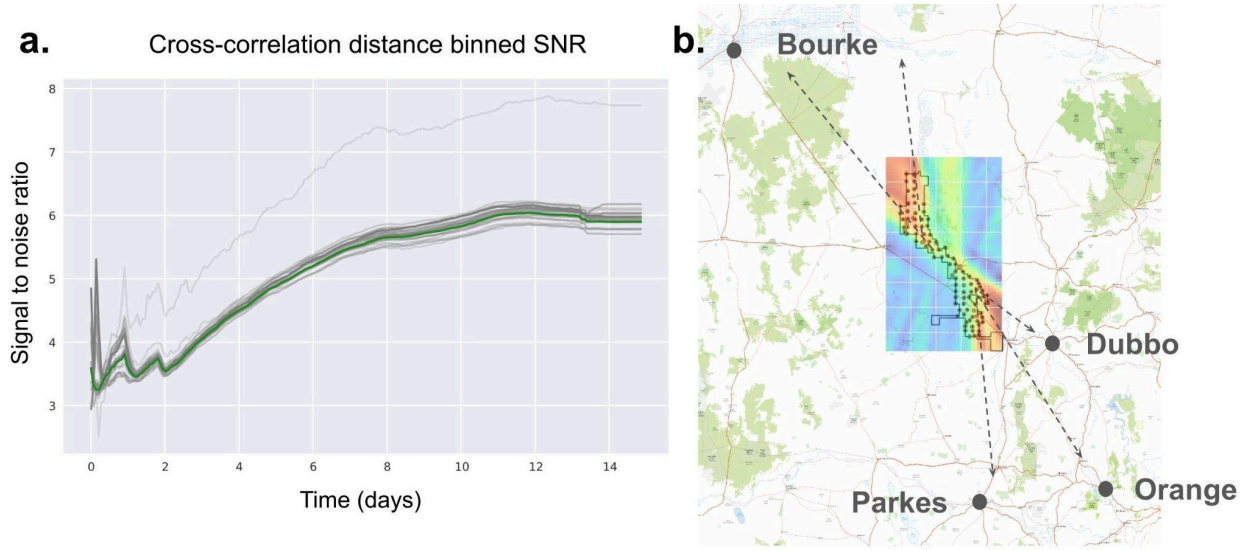

Figure 6. Ambient noise signal sources. **a.** SNR evolution plot for distance binned CCFs showing convergence to a stable SNR = 6 after approximately 12 days. **b.** Beamforming plot for frequency 0.35Hz showing the azimuth of seismic noise sources with topographic map of survey district showing the locations of likely noise sources - population centres and major highways.

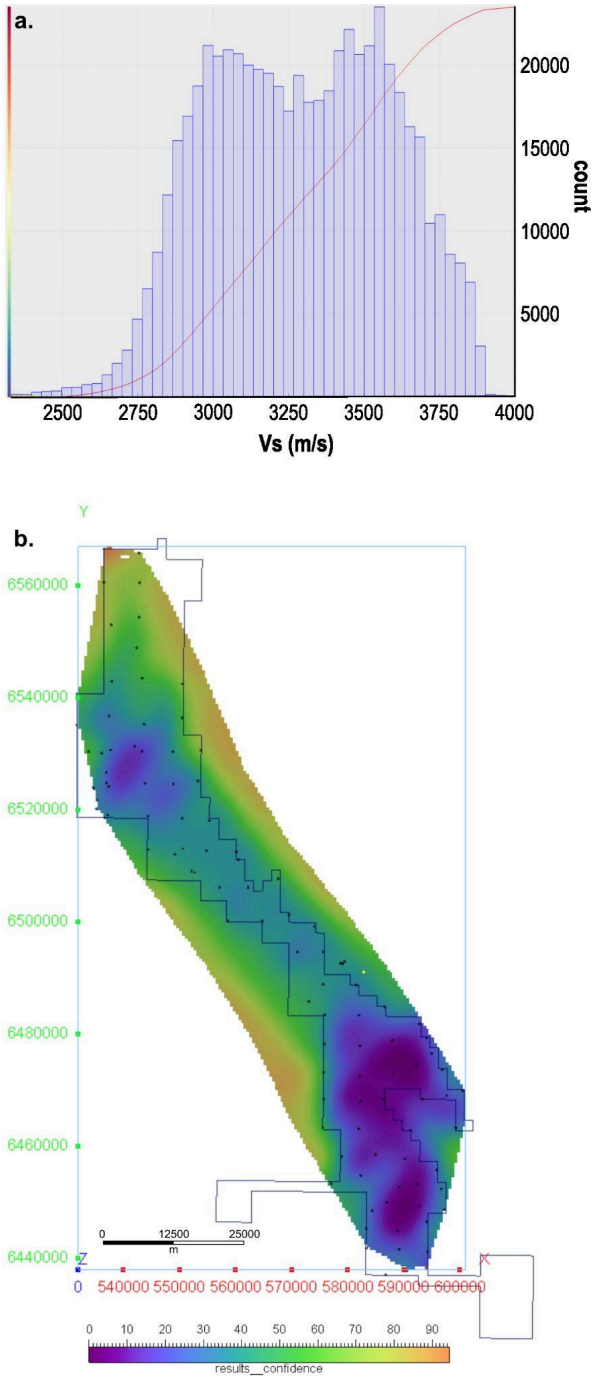

Figure 7. Features of the ANT velocity model. **a.** Distribution of velocities for each cell within the ANT velocity model. **b.** Confidence map for depth slice -2643m MSL, which is representative of the bulk model. Note that cooler colours indicate higher confidence, a measure which is largely based on the abundance of cross-correlated ray paths across the survey area.

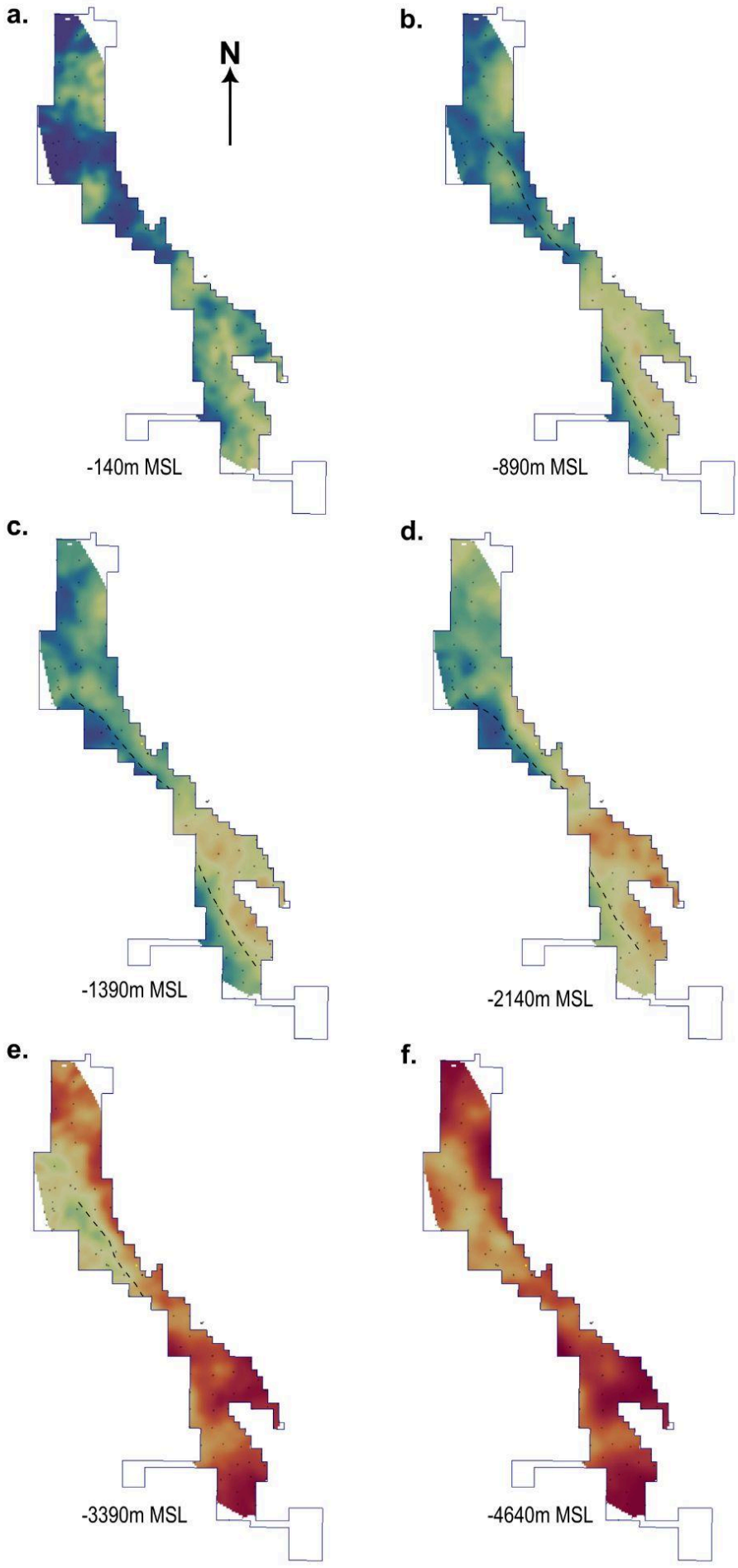
a.
N
-140m MSL
b.
-890m MSL
c.
-1390m MSL
d.
-2140m MSL
e.
-3390m MSL
f.
-4640m MSL

Figure 8. Depth slices through the 3D velocity model, clipped to tenement boundaries. Black dots show Geode locations. Dashed line indicates location of major northwest trending discontinuity Depths given as metres below mean sea level. **a.** -140m MSL. **b.** -890m MSL. **c.** -1390m MSL. **d.** -2140m MSL. **e.** -3390m MSL. **f.** -4640m MSL.

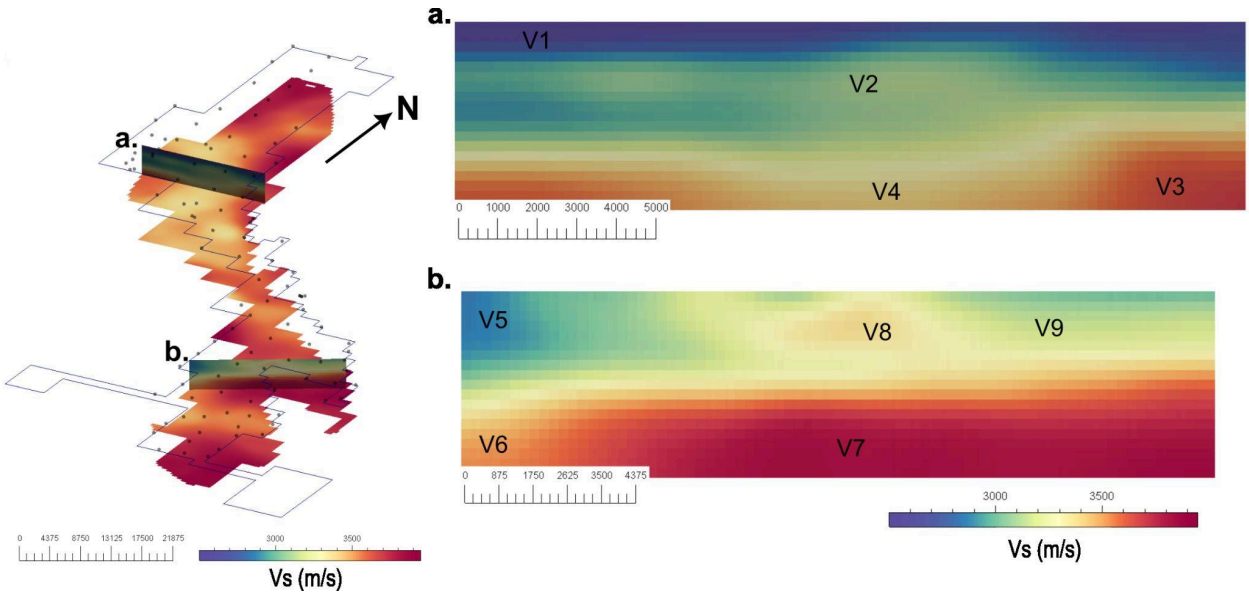

Figure 9. Example cross sections through 3D velocity model, clipped to tenement boundaries. Black dots show Geode locations. **a.** Cross section through the northern area of the model. **b.** Cross section through the southern area of the model. Note the slight variation in colour between the two sections is a result of shading applied by Geoscience Analyst to 3D objects based on the apparent sun angle. The velocities for each section are identical. Areas on each section marked V1, V2 etc, are discussed in the text.

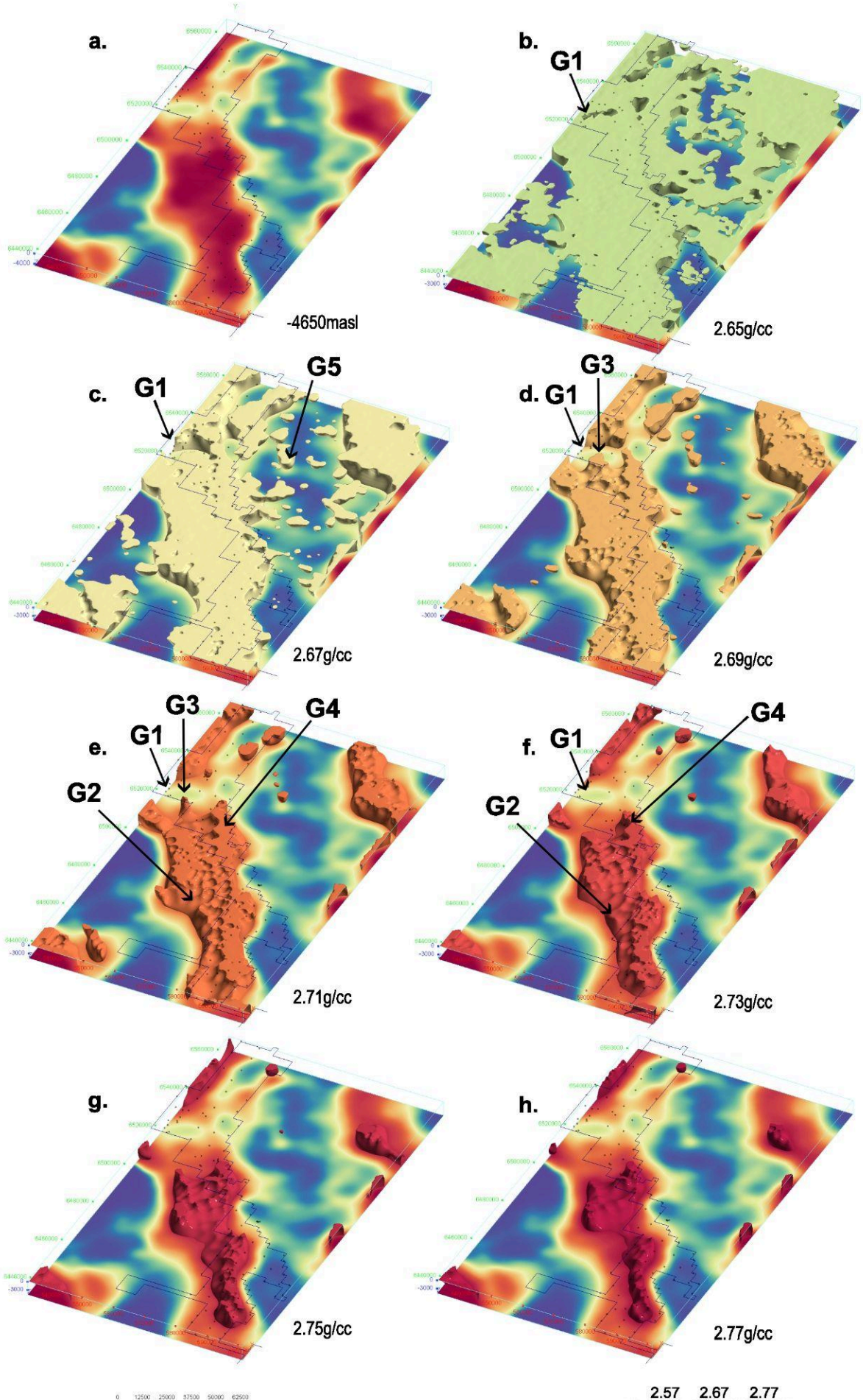
a.
-4650masl
b.
G1
2.65g/cc
c.
G1
G5
2.67g/cc
d.
G1
G3
2.69g/cc
e.
G1
G3
G4
G2
2.71g/cc
f.
G1
G4
G2
2.73g/cc
g.
2.75g/cc
h.
2.77g/cc
0 12500 25000 37500 50000 62500
2.57 2.67 2.77

Figure 10. Isosurfaces of the gravity inversion model. The isosurfaces are shown with reference to the contiguous tenement outline of the survey area and the location of the Geodes from which the ANT survey was undertaken. The isosurfaces are also shown with reference to **a.**, the -4650m MSL slice through the gravity model which forms a 2D backdrop to the 3D isosurfaces. **b.** 2.65 g/cc isosurface. **c.** 2.67 g/cc isosurface. **d.** 2.69 g/cc isosurface. **e.** 2.71 g/cc isosurface. **f.** 2.73 g/cc isosurface. **g.** 2.75 g/cc isosurface. **h.** 2.77 g/cc isosurface.

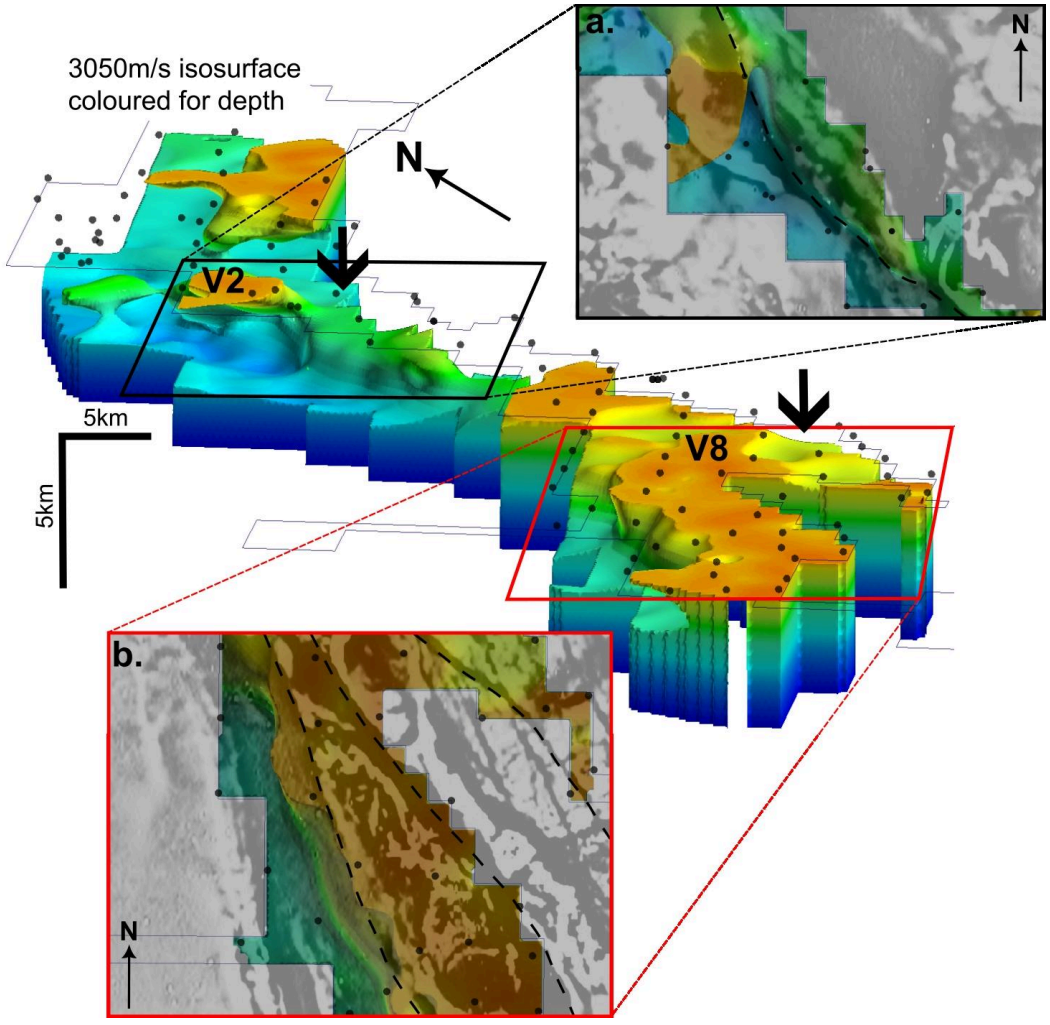

Figure 11. 3D ANT velocity model with emphasis on the major northwest-trending shear zone within the survey area. The 3050m/s isosurface is shown for reference and here is coloured orange to blue with depth. The vertical exaggeration is 2:1 to emphasise the vertical structure of the shear zone itself. The two areas highlighted, **a.** and **b.**, are zones where the shear zone is well expressed in the ANT velocity model. These zones are also shown in a top-down view (as indicated by bold arrows) with the 1st vertical derivative of reduced to pole total magnetic intensity grid (Geological Survey of New South Wales data) and dashed lines to show the trace of the shear zone in the magnetic data.

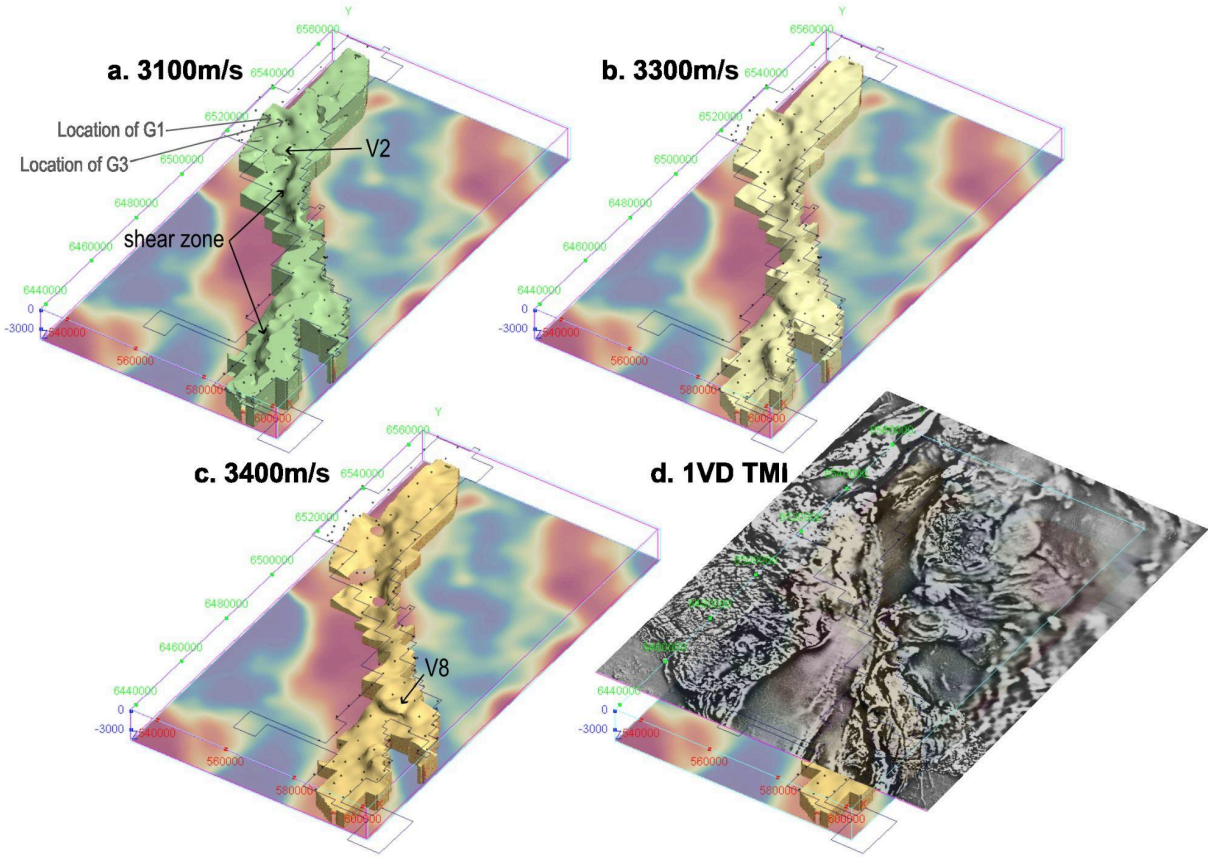

Figure 12. Oblique view towards the north-west across the ANT survey area showing isosurfaces of the velocity model and key features discussed in the text. Note the velocity model is shown with a 2x vertical exaggeration in order to accentuate vertical features in the model. Gravity grid is shown as the base layer in the image. **a.** 3100 m/s isosurface. **b.** 3300 m/s isosurface. **c.** 3400 m/s isosurface. **d.** 1st vertical derivative reduced to pole total magnetic intensity grid for the area (Geological Survey of New South Wales data) .

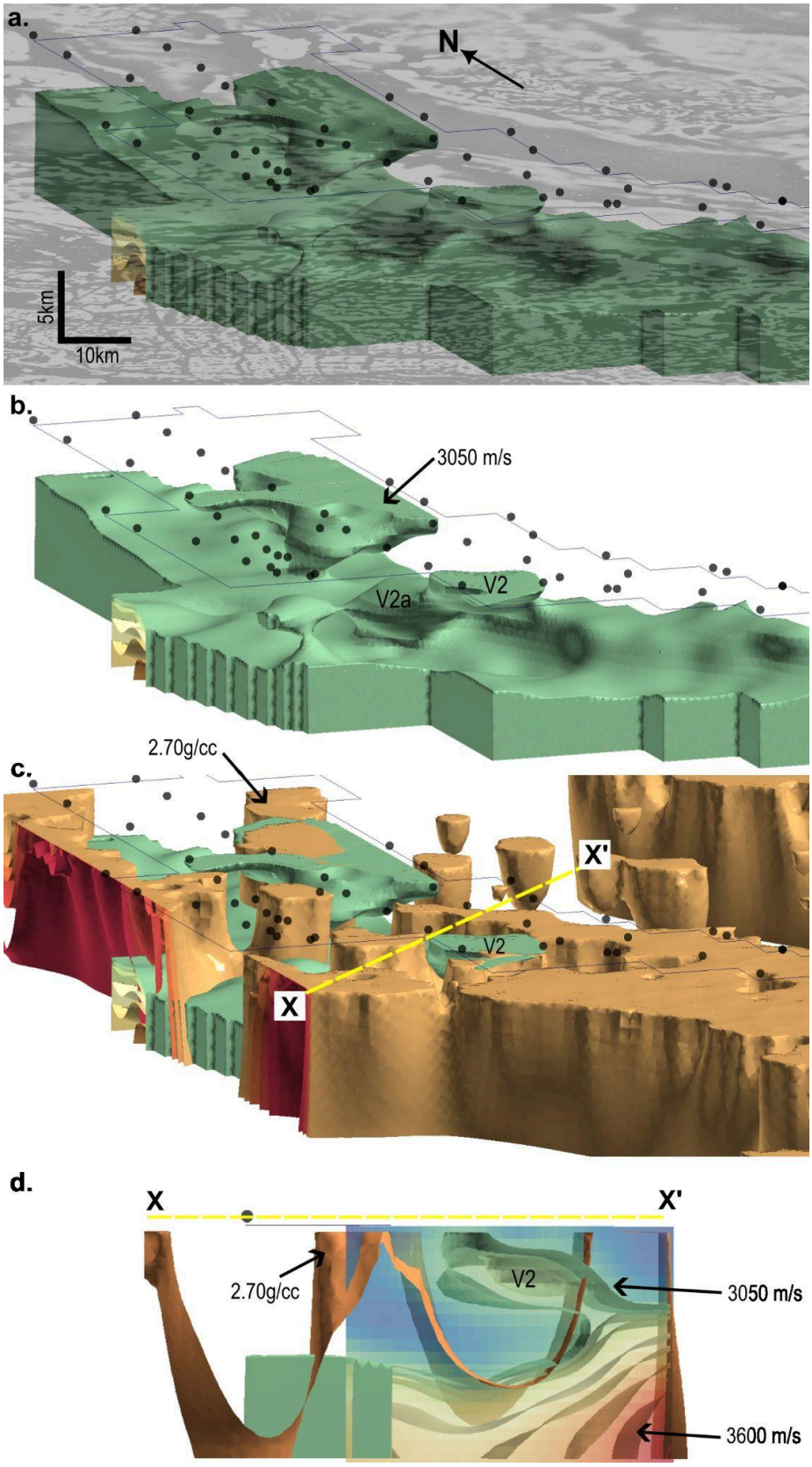
a.
N
5km
10km
b.
3050 m/s
V2a
V2
c.
2.70g/cc
X'
V2
X
d.
X
X'
2.70g/cc
V2
3050 m/s
3600 m/s

Figure 13. Detail of the ANT velocity model, gravity model in the northern region of the survey area in the vicinity of the velocity feature V2, with respect to the 1st vertical derivative total magnetic intensity grid across the region. Note that vertical exaggeration of 2x has been applied to the image to accentuate the shape of the velocity and gravity features. Fleet Geodes are shown as black dots, and outline of Inflection Resources tenement holding is also shown for reference. **a.** Oblique view of 1st vertical derivative of total magnetic intensity grid (Geological Survey of New South Wales data) with a transparency to show the underlying velocity and gravity model surfaces. **b.** Oblique view of velocity isosurface at 3050 m/s to accentuate the geometry of the plutonic bodies that are imaged in the model. **c.** Oblique view of velocity isosurface at 3050 m/s and gravity isosurface at 2.70 g/cc. **d.** Example cross section looking northwest through ANT velocity model and gravity inversion, showing the various isosurfaces of the velocity model from 3050 m/s to the deeper, higher velocity isosurface of 3600 m/s and juxtaposed against the 2.70 g/cc isosurface of the gravity inversion. The background section shows a slice through the ANT velocity model for reference. The location of the section X-X' is given in c. for reference.

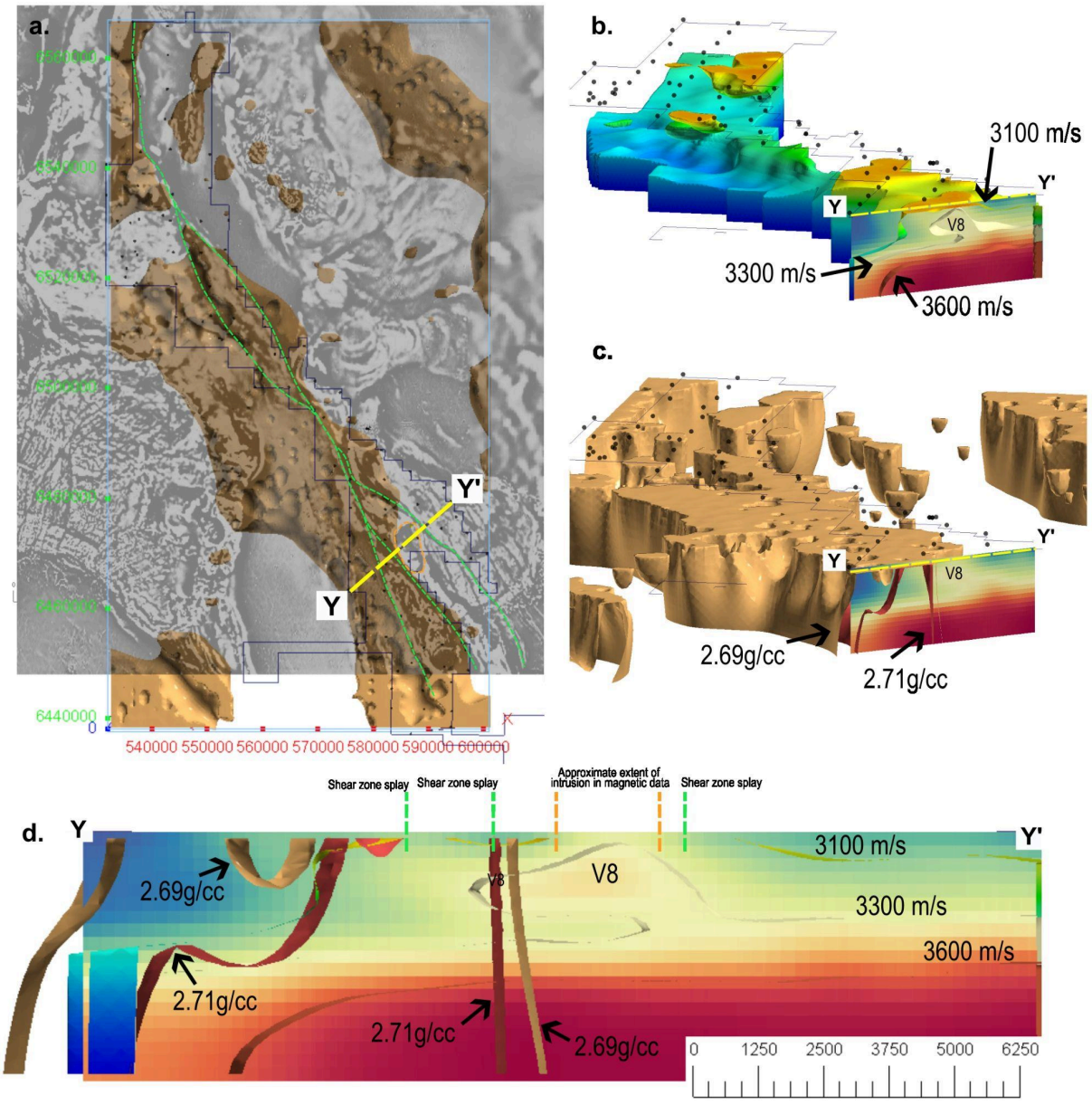

Figure 14. Detail of the southern portion of ANT survey area showing oblique and section views to highlight velocity feature V8. **a.** 1st vertical derivative reduced to pole total magnetic intensity grid for the area (Geological Survey of New South Wales data) with the 2.69 g/cc isosurface of the gravity model underlain to emphasise the location of the shear zone splays and the cross section. Note that vertical exaggeration of 2x has been applied to the image to accentuate the shape of the velocity features. **b.** Oblique view of the 3100m/s isosurface, coloured by depth from shallow (orange) to deep (blue) with a cross section shown through the velocity feature V8. The cross section shows the velocity model for reference. Note that vertical exaggeration of 2x has been applied to the image to accentuate the shape of the velocity features. **c.** Same view as in b., with

the gravity isosurfaces of 2.69 g/cc and 2.71 g/cc. **d.** Cross section, looking northwest approximately perpendicular to the strike of the main shear zone splays with outlines of selected velocity and gravity isosurfaces as indicated. The approximate location of the magmatic body indicated in the magnetic data is shown, along with the location of the shear zone splays for reference. No vertical exaggeration has been applied in this cross section.

Table 1. Summary of Geolibrary layer depth and shear wave velocity parameterisation applied to the ANT data for this survey.

Layer #	Vs min (m/s)	Vs max (m/s)	Layer Vs (m/s)	Layer mid depth (m)	Layer depth variation (m)
1	500	2500	uniform: (min, max)	Depth power law **	+- 30%
2-9	Vs power law *	4000	uniform: range +/- 50% previous layer Vs	Depth power law **	+- 30%
10	layer 9 Vs	4500	uniform: range +/- 50% previous layer Vs	N/A (halfspace)	N/A (halfspace)

** Vs power law function of layer Vs_min:* $Vs = 600 \times (layer\ number)^{0.3}$

*** Depth power law function of relative layer depth:* $layer\ depth = maxdepth \times \left(\frac{layer\ number}{total\ layers} \right)^{1.6}$